MOBILITY & VEHICLE MECHANICS

https://doi.org/10.24874/mvm.2024.50.04.02
UDC: 629.113.012.816:608.2

VEHICLE STABILITY ENHANCEMENT BASED ON WHEELS TORQUE DISTRIBUTION CONTROL FOR AN ACTIVE DIFFERENTIAL WITH ELECTROMECHANICAL ACTUATORS

Eid S. Mohamed[1,2]*

Received in December 2024 *Accepted in December 2024*

RESEARCH ARTICLE

ABSTRACT: High-performance vehicles use active differentials (AD) to maximize traction, stability, and safety by optimizing the torque distribution on the driving vehicle wheels. This work presents the torque distribution and speeds which are theoretically analyzed using mathematical models of the vehicle, driver, tire and drive train with an AD including the electromechanical actuation. The proposed controller is investigated using MATLAB/Simulink with AD as an external torque by an electromechanical actuation in a variety of driving scenarios, including straight lines under NEDC and J-turn input test with different road adhesions, to regulate lateral slide slip and vehicle yaw rate (YR) on different road adhesions can be obtained by an LQR controller. The results show that the AD can enhance the overall performance of the vehicle dynamics properties by transferring torque between the right and left wheels, which produces the direct yaw moment. The AD with integrated YR and vehicle side slip (VSS) control effectively improves vehicle dynamics and stability under different road maneuvers and adhesions.

KEY WORDS: *Active differential, motion stability, wheels torque distribution, yaw moment control, electromechanical actuators.*

[1] *Eid S. Mohamed, Faculty of Engineering, Mechanical Eng. Dept., Al-Baha University, KSA*
[2] *on Leave from Faculty of Engineering, Automotive dep., Helwan University, Egypt,*
e.mohamed@bu.edu.sa, *eng_eid74@yahoo.com* *-(*Corresponding author)*

POBOLJŠANJE STABILNOSTI VOZILA ZASNOVANO NA KONTROLI RASPODELE OBRTNOG MOMENTA TOČKOVA NA AKTIVNOM DIFERENCIJALU SA ELEKTROMEHANIČKIM AKTUATORIMA

REZIME: Vozila visokih performansi koriste aktivne diferencijale (AD) da maksimiziraju vuču, stabilnost i sigurnost optimizacijom raspodele obrtnog momenta na točkovima pogonskog vozila. Ovaj rad predstavlja raspodelu obrtnog momenta i brzine koje su teorijski analizirane korišćenjem matematičkih modela vozila, vozača, pneumatika i pogonskog sklopa sa AD uključujući i elektromehaničku aktivaciju. Predloženi kontroler je istražen korišćenjem MATLAB/Simulink-a sa AD kao eksternim obrtnim momentom elektromehaničkim aktiviranjem u različitim scenarijima vožnje, uključujući prave linije pod NEDC i J-turn ulaznim testom sa različitim adhezijama na putu, da bi se regulisalo bočno klizanje i skretanje vozila stopu (IR) na različitim adhezijama na putu može da dobije LKR kontroler. Rezultati pokazuju da AD može poboljšati ukupne performanse dinamičkih svojstava vozila prenosom obrtnog momenta između desnog i levog točka, što proizvodi direktan moment skretanja. AD sa integrisanom IR i kontrolom bočnog klizanja vozila (VSS) efikasno poboljšava dinamiku i stabilnost vozila pri različitim manevrima i prianjanjima na putu.

KLJUČNE REČI: *Aktivni diferencijal, stabilnost kretanja, raspodela obrtnog momenta točkova, kontrola momenta skretanja, elektromehanički aktuator*

VEHICLE STABILITY ENHANCEMENT BASED ON WHEELS TORQUE DISTRIBUTION CONTROL FOR AN ACTIVE DIFFERENTIAL WITH ELECTROMECHANICAL ACTUATORS

Eid S. Mohamed

INTRODUCTION

- ***Background of vehicle stability***

Most vehicle dynamic control systems available on the market are brake-based and apply individual wheel braking forces using anti-lock braking system hardware to preserve vehicle stability in emergencies. These dynamic stability control (DSC) systems employ differential tire brake forces between the vehicle's wheels to generate the required yaw moment for correction. These systems are highly effective when the handling limit is approached, but they are undesirable for everyday driving conditions due to the control action's direct impact on the longitudinal dynamics of the vehicle, which affects the vehicle's longitudinal performance and distracts the driver [1, 2]. Early research on active safety and vehicle stability systems mostly concentrated on enhancing the motion's longitudinal dynamics, namely on more efficient traction control (TC) and anti-braking (ABS) systems active front steering (AFS) systems and yaw motion control (YMC). By optimizing the tractive and the tire and the road's lateral forces, (LSD) systems not only keep the wheel from slipping but also increase vehicle stability and steerability [3,4]**.** To maintain vehicle stability in harsh handling conditions, an AD design approach and rescheduled active steering control were created. The effectiveness of the chosen modeling and controller design methods in enhancing the ability of the vehicle to handle when cornering on roadways by reducing the lateral forces between the tire and the pavement with different adhesion coefficients and during variable-speed operations was demonstrated through simulations [5, 6]**.**

- ***Overview of an active differential***

Other actuation technologies that can offer more stability without the obtrusiveness of a brake-based system are being explored. One such option is active limited slip differentials (ALSDs), which provide electronically regulated torque transfer between the driven wheels. By generating a yaw moment through controlled torque transfer across an axle, vehicle stability can be increased. This increase in stability can be accomplished less invasively than with a brake-based control system because wheel torque is reapportioned rather than decreased. An automotive differential mechanism's primary function is to prevent the traction wheel from slipping when the car turns a bend. This function is often carried out using a planetary gear, which maintains an equal torque distribution while permitting varying rotational speeds to the wheels to which the differential is linked.

Compared to a regular differential, a limited slip differential might (LSD) have numerous advantages. By biasing torque to the wheel with superior traction, LSD helps improve the overall traction and handling performance of the vehicle. This can be especially beneficial in situations such as driving on slippery or uneven surfaces, where one wheel may lose traction more easily than the other. Better handling and mobility qualities may result from this. Because of their design, traditional LSD has inherent restrictions. Any vehicle's mobility and handling can be maximized by electrically regulating the differential's output **[7-9].** Companies in the automotive industry and literature have long recognized the impact of LSD on the dynamics of the vehicle. The industry has long adopted passive self-locking mechanisms. The automotive industry and businesses have undertaken numerous initiatives in recent years to use regulated, semi-active, or ADs to get around these restrictions **[10, 11].**

Limited slip differentials (LSDs), which can provide an internal locking torque that enables the differentiation of the torque output and the generation of a yaw moment on the vehicle, are key characteristics of torque distribution systems. By dynamically adjusting the torque distribution, controllable LSD can enhance vehicle stability and cornering performance. For example, during cornering, if the inside wheel loses traction and starts to spin, the LSD can transfer more torque to the outside wheel, which has better grip. This helps to prevent excessive wheel spin and maintain traction, allowing the vehicle to effectively and safely navigate the turn. Furthermore, controllable LSD can also help to mitigate under steer and over steer tendencies. Under steer occurs when the front wheels lose grip and the vehicle tends to push wide in a turn. By transferring more torque to the rear wheels, controllable LSD can increase rear traction and improve cornering performance. [12, 13]. Adaptive systems known as magnetorheological (MR) devices can change their characteristics by applying a regulated magnetic field with an electrical power signal. To achieve this goal, countless attempts have been made to create LSDs and their control systems to satisfy the Figure 1 shows the classification of clutch types, they can be roughly categorized as electromagnetic clutches, pneumatic clutches and brakes, hydraulic clutches, and mechanical clutches. These uses clutches mechanically, hydraulically, pneumatically, and electromagnetically, as their names imply.

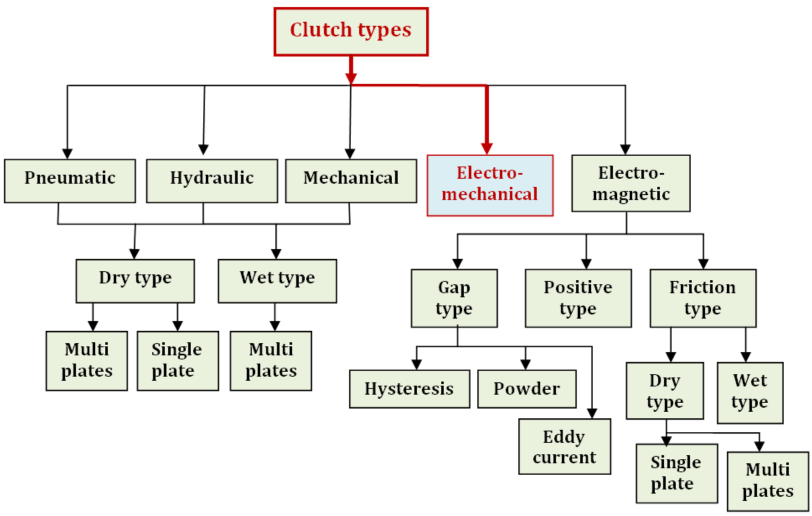

Figure 1: Classification of clutch types

Figure 2 shows the diagram of a conventional differential (CD) and active differential (AD), a CD is a fixed distribution of the drive torque with a conventional rear differential; a conventional rear differential consists of an angled drive and a differential gear and always distributes the drive torque equally (50:50) to both sides. Different rotational speeds are balanced out. The other gear ratios for the various vehicle models are achieved by the different number of teeth on the drive pinion and crown gear. The speed of the drive wheels can differ from each other because of the various distances they cover when cornering. The drive torque is always distributed equally to both drive wheels and does not therefore generate any yawing.

These benefits are counterbalanced by a major disadvantage if the tire-road adhesion is different at the two wheels. The propelling forces that are to be transferred to the road are then limited to the lower of the two potential adhesion levels at the drive wheels. If the adhesion ratio is unfavorable on one side, it means that a vehicle (without electronic dynamic driving system) would not be able to move off. The drive torque would be converted into useless rotational acceleration for the wheel with the lower potential adhesion level, while the higher potential adhesion of the second drive wheel remains unexploited. The AD with distribution of the drive torque by the rear differential with mechanical locks (limited-slip differential).

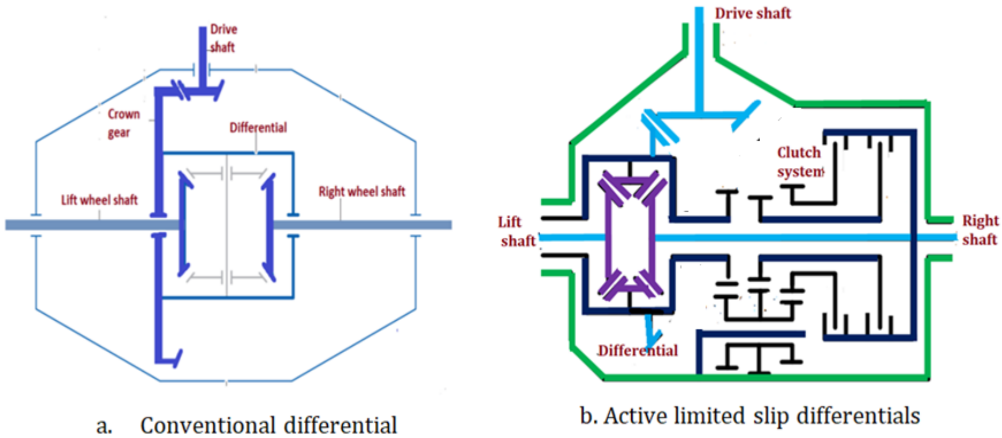

Figure 2: Schematic diagram of a CD and AD

1. VEHICLE DRIVE TRAIN MODEL

The torque generated by the ICE engine and sent to the vehicle's drivetrain via AD is represented by T_e in Figure 4.The friction torques (T_{cr} and T_{cl}) are represented as simple Coulomb friction proportional to the clutch compression force (F_{cr} and F_{cl}). By imposing the dynamic equilibrium of the planetary and solar gears, differential housing, gearbox, and rotary engine components, the equilibrium differential equations characterizing the AD dynamics were found using both Lagrange and Newton techniques. The dynamic equations are reduced to only three by applying the standard kinematic relations between the angular velocities of the solar, planetary, and differential housing gears. These formulas allow the motor torques (T_{rs}, T_{ls}) and angular velocities (ω_r, ω_l) on the left and right solar gear. The vehicle dynamic equilibrium equations:

$$J_e \ddot{\theta}_e = T_m - T_t \tag{1}$$

$$J_t \ddot{\theta}_t = T_t - T_p \tag{2}$$

$$J_g \ddot{\theta}_g = I_g T_p - T_d \tag{3}$$

$$J_d \ddot{\theta}_d = I_d T_d - (T_{wl} + T_{wr}) \tag{4}$$

$$J_{eq}\ddot{\theta}_{ax} = (T_{wl} + T_{wr}) - (F_{wl} + F_{wr})R_w - (F_{cl} + F_{Cr})R_p \tag{5}$$

where $\ddot{\theta}_e$, $\ddot{\theta}_t$, $\ddot{\theta}_g$, $\ddot{\theta}_d$, and $\ddot{\theta}_{ax}$ are the angular accelerations of the engine output shaft, torque converter axles, planetary gear box, differential gear and axle of drive wheels. J_e , J_t, J_g, J_p, J_d, and J_{eq}, are moment of inertia of the engine, torque converter axles, planetary gear, differential gear and axle of drive wheels components. T_e, T_t, T_p, T_d, T_{wl}, *and* T_{wr} are the engine torque, torque converter torque, planetary gear torque, differential gear torque, left and right wheels torque. F_{wl}, *and* F_{wr} are the left and right wheels force. F_{cl}, F_{cr} are the left clutch force and right clutch force of the AD. I_g, I_d are the transmission ratio in gearbox and the final drive ratio.

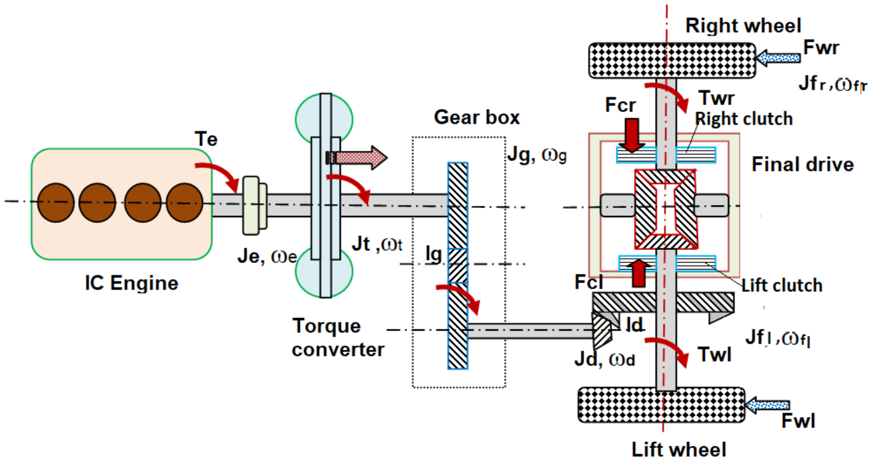

Figure 3: The vehicle driveline model

1.1 Engine model

The engine is represented model as the torque actuator, the model constant inertia that is coupled to the flywheel and clutch via the crankshaft. The engine's net torque, taking friction and torque losses into account, is represented as torque T_e. The engine model is derived from existing experimental data and is quasi-static. A look-up table is used to derive engine torque as a function of engine throttle position, as seen in **Table 1**.

Table 1: *IC Engine torque map*

Engine torque (N.m)		**Throttle position (θ %)**							
		5	**10**	**15**	**20**	**25**	**30**	**40**	**50**
Engine speed (***Ne*** rpm)	**100**	65	80	90	117	109	110	118	125
	1500	70	96	100	132	133	134	136	140
	2000	60	110	120	133	141	142	144	150
	2500	45	87	102	133	147	148	150	155
	3000	36	74	99	133	153	159	168	165
	3500	22	60	88	136	152	161	175	178
	4000	12	55	83	126	150	160	177	182

	4500	9	51	77	140	155	179	186	199
	5000	5	43	75	136	175	194	205	220
	5500	0	33	71	101	147	167	185	200
	6000	0	22	68	94	136	161	160	193
	6500	0	**18**	**66**	**88**	**130**	**140**	**155**	178

1.2 Torque converter model

A centripetal impeller and turbine with a lock-up clutch serves as the torque converter in power train. The following criteria are used to assess the torque converter transmission characteristics:

$$\omega_t = i_s \omega_b \tag{6}$$

$$T_b = \lambda_b \rho g \omega_b^2 D^5 \tag{7}$$

Where ω_t and ω_b are turbine and impeller speeds and, T_b is impeller torque, λ_b is torque capacity coefficient of torque converter, ρ is oil density, η_t is the transmission efficiency.
The power loss (P_t) is expressed by:

$$P_t = T_b \omega_b (1-\eta_t) \tag{8}$$

1.3 Active differential model

An electronically controlled system regulates the torque distribution between the left and right wheels of the driving axle, limited slip differential. Limited slip functionality is provided via a multi-plate dry clutch positioned between the differential enclosure and the output shaft. Clutch engagement starts the torque transfer from the housing to the output shaft. This makes it possible to individually modify the torque magnitude of each output shaft. The clutch torque needs to be changed to produce the appropriate vehicle yaw dynamics under particular driving circumstances.
A Simple diagram of an AD is shown in **Figure 4** for easy comprehension. Electromechanical actuators activate the friction plates. T_g represents the input driving torque that is transferred to the differential by the gearbox, whilst T_{wr} and T_{wl} represent the torques at the output to the left and right shafts, respectively.

$$T_{wr} = \frac{T_g - T_{cr} + T_{Cl}}{2} \quad and \; T_{wl} = \frac{T_g - T_{cl} + T_{Cr}}{2} \tag{9}$$

The variation in torque between the clutches on the left and right is known as the controller output torque (T_{diff}.)

$$T_{deff} = T_{Cr} - T_{Cl} \tag{10}$$

Where $T_{cr} = F_{cr} R_p$ *and* $T_{cl} = F_{cl} R_p$

The subsystem was dedicated to specific driving conditions, like starting on the AD. In this situation, the adhesion of one driven wheel is low (low ϕ) surface, such as ice or mud, and it is unable to transmit the driving torque to the earth.. All of the driving power would be dispersed by a free differential while the automobile is stationary by allowing the wheel on low ϕ to spin (**Figure 5**).

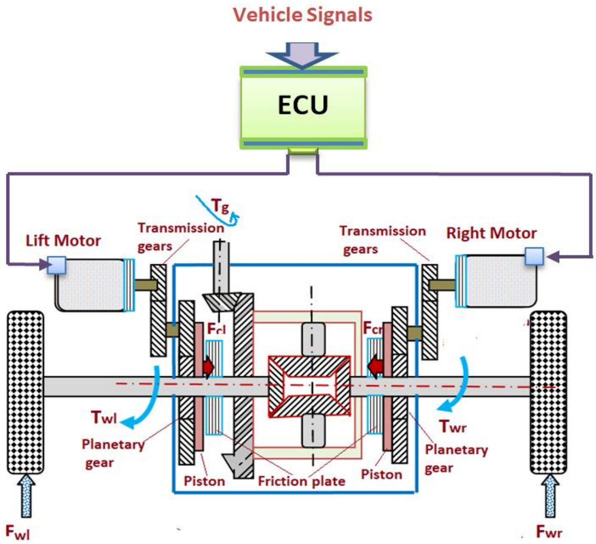

Figure 4: *A Simple diagram of an active diff*erential

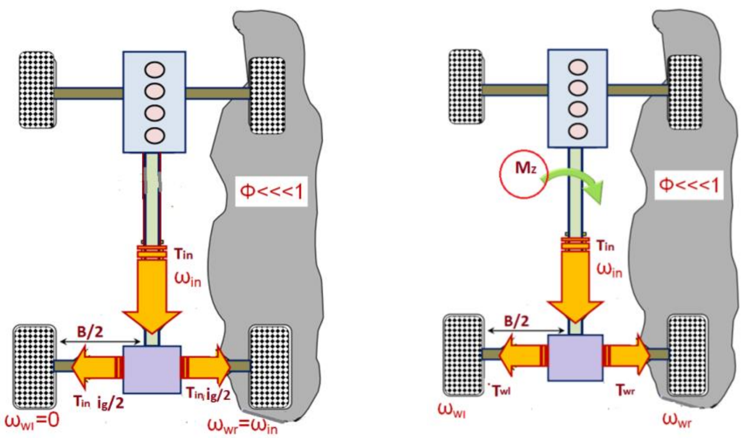

a. Free differential

b. Active differential

Figure 5: *Working principle of free and active differential*

1.4 Electromechanical actuator model

A DC motor's electrical circuit is made up of a voltage source (the controller provides the voltage input), a resistor, an inductor, and a back EMF that is proportionate to the motor's RPM connected in series. An electromechanical actuator (EMA) regulates the speed ratio, and the DC motor's power consumption is stated in:

$$P_m = \frac{V_o I_o}{\eta_m} \tag{11}$$

2.

where P_m denotes power consumed by the DC motor, V_o operating voltage of the motor, I_o operating current, and η_m charge–discharge efficiency of the battery. A DC motor with a permanent magnet is selected as the actuator motor of the EMA's. Additionally, the formulae for torque and voltage balancing are explained in Eqs. (5) and (6), respectively, as follows

$$V = IR + L\frac{dI}{dt} + K_e\omega_m \tag{12}$$

3. $$J_m\frac{d\omega_m}{dt} = K_T I - T_L \tag{13}$$

4.

where R is the DC motor armature resistance, L is motor armature inductance, K_e is back-EMF coefficient, J_m is the output shaft moment of inertia, ω_m is the output shaft angular velocity, K_T is the torque coefficient, and T_L is the DC motor torque load.

2 VEHICLE DYNAMIC MODEL

A 4-wheel vehicle handling model that accounts for tire non-linearity and vehicle roll dynamics must be developed because handling studies of standard AD systems usually use a road vehicle bicycle model, which ignores lateral load shift and tire saturation limit. Make use of the coordinate system for vehicles depicted in **Figure 6 (a).**

Front, Right wheel $F_{fr} = W_f - \frac{ma_x h_{cg}}{2L} + \frac{ma_y h_{cg} b}{2T_f L}$

Front, Left wheel $F_{fl} = W_f - \frac{ma_x h_{cg}}{2L} - \frac{ma_y h_{cg} b}{2T_f L}$ (14)

Rear, Right wheel $F_{rr} = W_r + \frac{ma_x h_{cg}}{2L} + \frac{ma_y h_{cg} a}{2T_r L}$

Rear, Left wheel $F_{rl} = W_r + \frac{ma_x h_{cg}}{2L} - \frac{ma_y h_{cg} a}{2T_r L}$

The traction force distribution is described as a four-wheel model with three degrees of freedom: longitudinal, lateral, and yaw. The following expression can be used to illustrate the equations that govern both lateral and longitudinal motion:

$$m\dot{V}_x = ma_x = \sum F_x = F_{xr} + F_{xl} \tag{15}$$

$$ma_y = F_{yfr}\cos(\delta_f) + F_{yfl}\cos(\delta_f) + F_{yrr} + F_{yrl} \tag{16}$$

$$mV(\dot{\beta} + \Omega) = \sum F_y = F_{yfr} + F_{yfl} + F_{yrr} + F_{yrl} \tag{17}$$

where m is the vehicle mass; a_x and a_y are the longitudinal and lateral accelerations of vehicle, respectively and δ_f is the front steering angle. The slip angle, Ω is the YR, F_{yfl}, F_{yfr} is the cornering force of the front tires, F_{yrl}, F_{yrl} is the cornering force of the rear tires, and V_x is the vehicle velocity.

2.1 Reference model

Based on earlier studies, a simplified two-DOF vehicle model is typically developed to explain the lateral dynamics of the vehicle, using the yaw rate Ω and the VSS angle β as the system's states. **Figure 6 (b)** displays the yaw plane reference model system. One way to characterize the 2DOF model is

$$\dot{\beta}=\left[-\frac{2(C_f+C_r)}{mV_x}\right]\beta+\left[-\frac{2(aC_f-bC_r)}{mV_x^2}-1\right]\Omega+\frac{2C_f}{m}\delta_f \tag{18}$$

$$\dot{\Omega}=\left[-\frac{2(aC_f-bC_r)}{I_zV_x}\right]\beta-\left[\frac{2(a^2C_f+b^2C_r)}{I_zV_x}\right]\Omega+\frac{2aC_f}{I_z}\delta_f+\frac{M_z}{I_z} \tag{19}$$

Equations for linear single-track models are:

$$\begin{bmatrix}\dot{\beta}\\ \dot{\Omega}\end{bmatrix}=\begin{bmatrix}\frac{2(C_f+C_r)}{mV_x} & \left[-\frac{2(aC_f-bC_r)}{mV_x^2}-1\right]\\ \left[-\frac{2(aC_f-bC_r)}{I_zV_x^2}-1\right] & \left[\frac{2(a^2C_f+b^2C_r)}{I_zV_x}\right]\end{bmatrix}\begin{bmatrix}\beta\\ \Omega\end{bmatrix}+\begin{bmatrix}0\\ \frac{1}{I_Z}\end{bmatrix}M_Z+\begin{bmatrix}\frac{2aC_f}{m}\\ \frac{2aC_f}{I_z}\end{bmatrix}\delta_F \tag{20}$$

The vehicle motion in longitudinal direction can be written as:

$$m\dot{V}_x=ma_x=\sum F_x=F_{xr}+F_{xl} \tag{21}$$

The computer simulation of YR tracking control is conducted in Matlab/Simulink, the vehicle parameters, drive line parameters and DC motor parameters used are taken on **Table 1.**

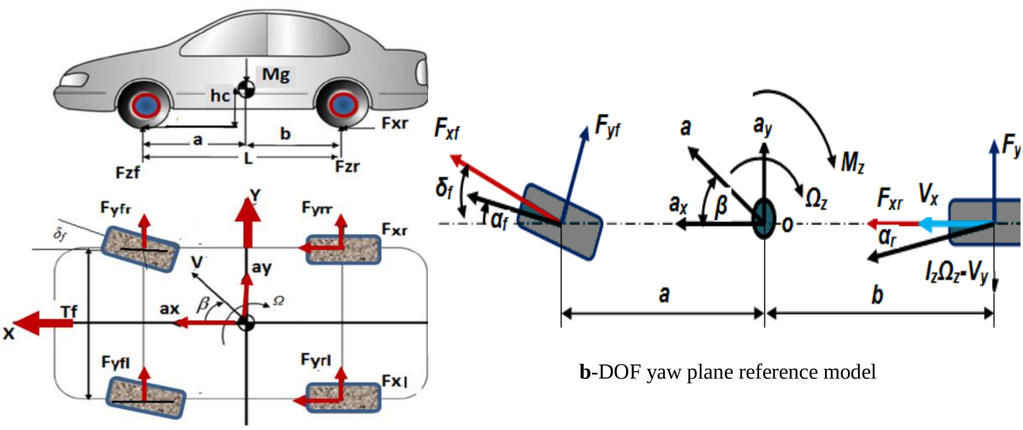

b-DOF yaw plane reference model

a. The vehicle coordinates and force analysis

***Figure 6**: Vehicle dynamic and reference models*

2.2 Vehicle path following Model

The single-track model and the state variables in terms of position and orientation error are used to create a dynamic path-following model. **Figure 7(a)** shows the configurations of the desired and actual vehicle orientations. The vehicle orientation on its intended path is represented by the x_d, y_d frame, whereas the x-y frame shows the vehicle orientation on its actual path **[21].** At the preview point, the anticipated lateral position is:

$$Y(t+t_p)=Y(t)+a_y\frac{t_p^2}{2}+V_x\Omega t_p \tag{22}$$

where, t_p denotes the driver preview time, $y(t+t_p)$ the predicted vehicle lateral position at the preview point, Ω vehicle yaw angle. The desired position vector R_d can be defined in the mobile frame x–y as:

$$\vec{R}_d = x_d\,\vec{i} + y_d\,\vec{j} \tag{23}$$

The goal is to minimize both the lateral position and orientation errors relative to the desired path, in order to provide a desired path control. The orientation error and its derivative can be written as:

$$\Delta\Omega = \Omega_{des} - \Omega_{act}$$
$$\Delta\dot{\Omega} = \dot{\Omega}_{des} - \dot{\Omega}_{act} \tag{24}$$

where $\dot{\Omega}_{des}$ is the rate of change of the desired orientation of the vehicle and is defined as:

$$\dot{\Omega}_{des} = \frac{V_x}{R_{des}} \tag{25}$$

where R_{des} is the radius of curvature of the desired path.

2.3 *Vehicle tyre model*

As seen in **Figure 7 (b)**, a simplified quarter car vehicle model experiencing a driving move or completely straight line regenerative braking has been taken into consideration. The torque equation for adaptive DYC are imposed by mean of appropriate motor actuators, the DYC is actuated through the rear axle tyres characteristic.

$$J_{wrl}\,\dot{\omega}_{rl} = T_{rl} - F_{xrl}.R_w$$
$$J_{wrr}\,\dot{\omega}_{rr} = T_{rr} - F_{xrr}.R_w \tag{26}$$

Where V_x represents the longitudinal velocity, ω_{rl}, ω_{rr} is the angular rotational speed of Left/right wheel, T_m represents the traction torque generated by the motor, R_w, J_w wheel radius, inertia momentum , $F_{x,rl}$, $F_{x,rr}$ Rear left/right tyre longitudinal forces, T_{rl}, T_{rr} Left/right wheel tractions

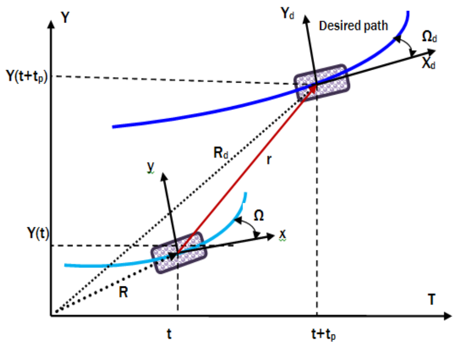

a. predictive driver model

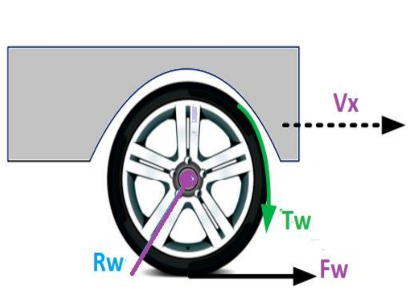

a. Single tyre model

Figure 7: *vehicle path and tyre models*

Using tyre magic formula, the actual longitudinal tyre force (F_{xi}) can be obtained. The tyre magic formula expresses the tyre longitudinal force (F_{xi}), the lateral force (F_{yi}), and the aligning torque (M_{zi}) as a function of the tyre side slip angle (α_i) and the longitudinal slip ratio (λ_i). The general form of the tyre magic formula is as follows **[16]:**

$$\begin{aligned} y(x) &= D\sin\left[C\tan^{-1}(Bx - E(Bx - \tan^{-1}(Bx)))\right] \\ Y(X) &= y(x) + S_v \\ x &= X + S_h \end{aligned} \tag{27}$$

the slip ratio (λ) can be rewritten as

$$\lambda = \frac{V_x - V_w}{V_x} = \frac{V_x - \omega.R_w}{V_x} \tag{28}$$

where the output variable $y(x)$ represents the tyre longitudinal force, lateral force, and aligning moment, and the input variable (x) may represent α_i or λ_i . The coefficient B is the stiffness factor, C the shape factor, D the peak factor, and E the curvature factor. S_h and S_v are the horizontal and vertical shifts, respectively. For a given tyre, using experimental data, these coefficients are tuned. These coefficients can be tuned easily by the genetic algorithm method. $Y(X)$ is a changed coordinate system to enable an offset with regard to the origin in the curve produced by the magic formula.

2.4 Design of control system

The goal of the control system to ensure the car travels along the intended route with side-slip angle and YR values that are almost at their intended levels by AD traction torque distributions. Furthermore, even when the driver directives are present, the controller must function as intended. An ideal controller with the construction depicted in **Figure 8** is created for this objective. It is divided into three sections: (YMC), driver dynamics, and vehicle dynamics.

2Optimal design

The Linear Quadratic Regulator (LQR) approach serves as the foundation for the control system that this research suggests. In this section, the best controller for a linear tracking problem is designed using the 6DOF linear vehicle model. For the purpose of controlling vehicle dynamics, the performance index usually takes the following basic form:

$$J = \frac{1}{2}\int_0^\infty \left[w_1(\Omega - \Omega_d)^2 + w_2 M_Z^2 + w_3 T_{diff}^2 + w_4 v^2 + w_5(\delta_f - \delta_d)^2\right]dt \tag{29}$$

where T_{diff} is the AD torque, M_z is the vehicle yaw moment, Ω_d is the desired YR, δ_d is the desired steering angle and w_1, w_2, w_3, w_4, and w_5 are the weighting parameters used to balance each term's relative relevance in the equation. The optimal control rule is composed of the disturbance feed-forward signal related to the road specification and the state variable feedback signal, which is represented as:

$$M_Z = K_\Omega \Omega + K_\delta \delta + K_\beta \beta + K_v v \tag{30}$$

where $K_\Omega, K_\delta, K_\beta$ and K_v are known as the state gains.

2.4.2 Path tracking control

The closed-loop system of driver/vehicle interaction for the path-tracking problem is finished using the driver model that is shown below. One widely used approach is to define human control behavior as a transfer function and treat it as a linear continuous feedback control. It is possible to justify PID controllers for this reason.

The transfer function of the driver model is given by **[16]**

$$Y(t+t_p) = Y(t) + a_y \frac{t_p^2}{2} + V_x \Omega t_p \tag{31}$$

The actual YR control techniques based on the existing control loop to accomplish the parking trajectory tracking function. The short steering angle control algorithm is presented in this section. The difference between the wheels slip command and vehicle body slip feedback is used by the controller to determine the AD motor current command. The linear 2DOF model of the dynamic system can be defined using the state space form that follows:

$$\begin{Bmatrix} \dot{x} = Ax + Bu \\ y = Cx \end{Bmatrix} \tag{32}$$

where

$x = [\beta \quad \Omega]^T$, $u = [\delta_f \quad M_z]^T$ and $y = [\Omega \quad a_y]^T$

where M_z indicates input of yaw moment control (YMC), It is produced by the AD motors' autonomous torque management., and δ_f is the steering angle.

The tracking error is represented by the variable *e*, which is given to the PID controller, which calculates the error between the actual output *Y(t)* and the desired input value $Y(t+t_p)$. The proportional gain (KP), integral gain (*KI*) and derivative gain (*KD*), the control gains are evaluated from error signal *e* will the signal *u* just past the controller **[7, 19]**

$$u = K_P e + K_I \int e\,dt + K_d \frac{de}{dt} \tag{33}$$

The values of KP=2500, KI=7.8, and KD=230 were chosen in order to achieve the necessary damping ratio, and each of these parameters was adjusted until the appropriate overall response was achieved.

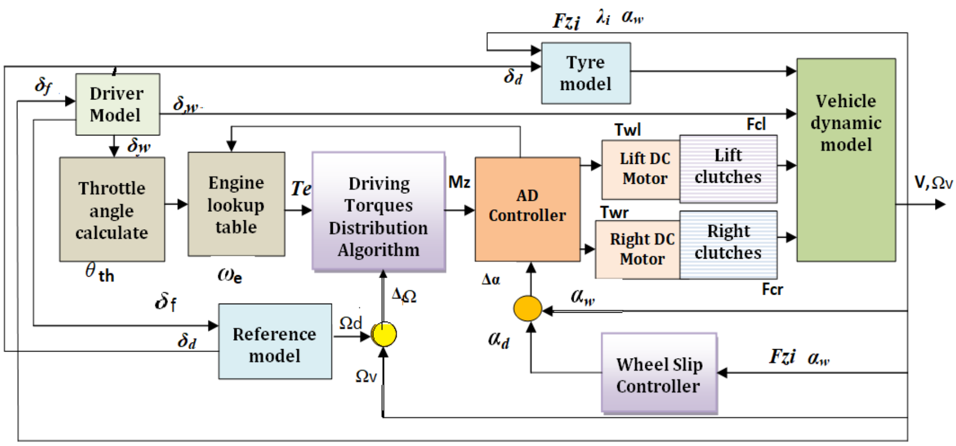

Figure 8: *Block schematic of the vehicle stability control system overall*

Table 2: Simulation model parameters

No.	Parameter	Notation	Unit	value
The parameters of vehicle model				
1	Sprung mass (mass vehicle)	m	kg	1300
2	moment of inertia about z axis	I_z	$Kg.m^2$	600
3	Wheel base	L	m	2.3
4	Distance of CG from front axle	a	m	1.15
5	Distance of CG from rear axle	b	m	1.26
6	Height of CG from ground	h_{cg}	m	0.4
7	Wheel radius	R_w	m	0.278
8	Track width axles	T	m	1.24
9	Cornering stiffness front and rear wheels	C_f C_r	N/rad	54000 35200
10	Max. motor torque at speed	T_{max}/N_e	Nm/rpm	210/5200
11	Tyre–wheel roll inertia	J_w	$kg\ m^2$	1.2
The driveline model				
1	Engine moment of inertia	J_e	$kg\ m^2$	4.98
2	Torque converter axles inertia	J_t	$kg\ m^2$	0.46
3	Planetary gear moment of inertia	J_p	$kg\ m^2$	0.26
4	Differential gear inertia	J_d	$kg\ m^2$	0.18
5	Gear transmission ratio	I_g	-	1
6	Final drive ratio	I_d	-	4
DC motor model				
1	moment of inertia	J_m	$kg\ m^2$	0,022
2	Maximum Current	I	A	200
3	Inductance	L	μH	18
4	Resistance	R	Ω	0.06
5	Torque coefficient	K_T	Nm/A	1.25
6	Back-EMF coefficient	K_e	V/rad/sec	0.5

3 SIMULATION RESULTS

There are two cases to discuss the results. First, the car is exposed to a road with a different friction between the right and left wheels, and the car drives in a straight line. Secondly, the car is exposed to a curved road. The typical curves of the lateral tire force in relation to tire VSS are displayed in **Figure 9** for different frictional road surface conditions, including dry asphalt (μ=0.8), dry cobblestone (μ=0.7), wet asphalt (μ=0.4), and snow (μ=0.2). In areas with a small tire slip angle (up to 4 degrees, for example), the lateral tire forces rise linearly as the slip angle increases. By adjusting the front steering angle, yaw stability can be improved.

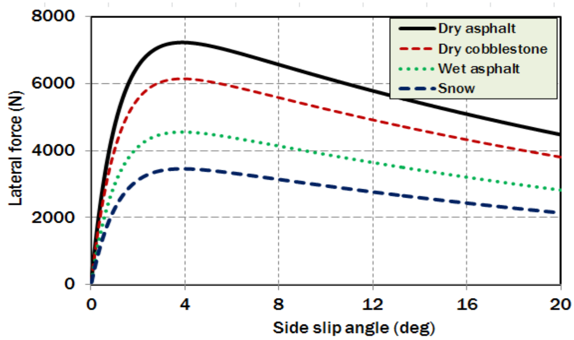

Figure 9: The tire lateral force characteristics with various road surfaces

3.1 Vehicle motion in straight line

The car underwent new European Driving Cycle testing (NEDC). Following the urban cycle, this one involves driving at a half-steady pace with occasional idling, accelerations, and decelerations. NEDC is made up of the urban driving cycle (UDC) and the extra-urban driving cycle (EUDC), which cover driving conditions on city streets and highways, respectively. UDC simulates an average speed of 18.9 km/h and a maximum speed of 60 km/h. A low-speed urban cycle lasting 780 seconds is repeated four times over the entire cycle, as shown in Figure. 10. With a mean speed of 63 km/h, the EUDC can reproduce a maximum speed of 120 km/h.

The vehicle power train is operated by a New European Driving Cycle (NEDC), which also determines the desired vehicle speed (V_d). A PID driver model is used to assess the throttle valve opening (θ_{th}) and pedal position (θ) by comparing the desired and actual vehicle speed (V) in order to choose engine (Ne-Te) operation values. In order to choose the best torque of wheels, an engine lockup table is utilized along with the real vehicle speed and engine characteristics (Ne-Te). The torque is expressed between left and right wheels according to AD motors torque.

The simulations presented in this section refer to a vehicle in straight line throughout the new European drive cycle (NEDC) with vehicle speed according to NEDC. Figure 10 shows the full cycle of NEDC input with four repetitions of a 780-second, low-speed urban cycle are made. With a mean speed of 63 km/h, the EUDC can reproduce a maximum speed of 120 km/h.

Figure 11 illustrates of the vehicle wheels torques and speed with dry asphalt (Φ=0.8) under NEDC. When all wheels of the vehicle are exposed to the same surface adhesion on dry asphalt, torque is distributed equally to the left and right wheels ($T_{wl}=T_{wr}$) see Figure 11 (a), and under the same conditions, the rotational speed of the right and left wheels is equal ($\omega_{wl}=\omega_{wr}$) see Figure 11 (b).

Figure 12 presents the vehicle wheels torque and speed with the CD with a slippery road. When the vehicle right wheels are exposed to a slippery road wet asphalt (μ=0.4) and the left one is exposed to a dry road dry asphalt (Φ=0.8), the rotational speed of the right wheels increases but the left wheels speed decreases, causing the car to become unstable.

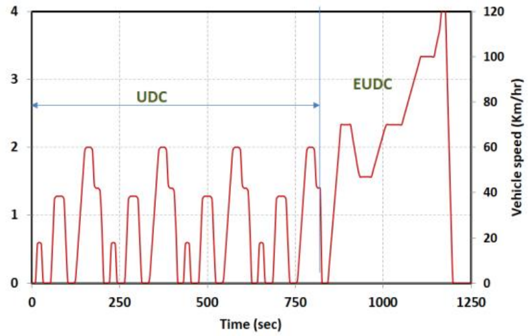

Figure 10: Vehicle speed curve.

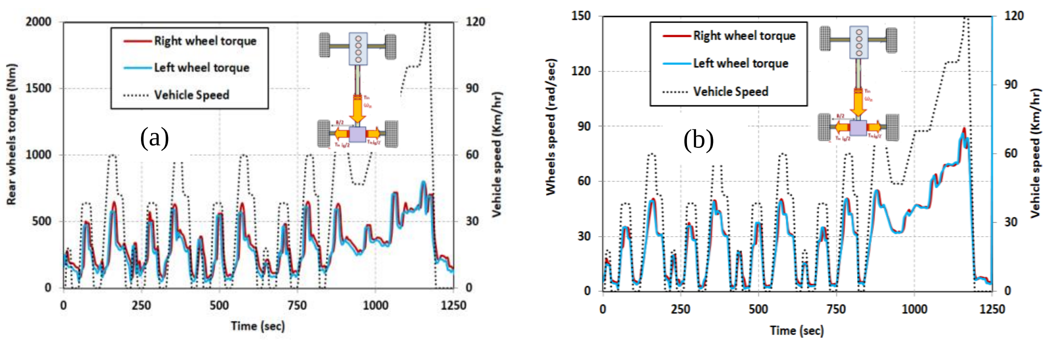

Figure 11: Vehicle wheels torques and speed.

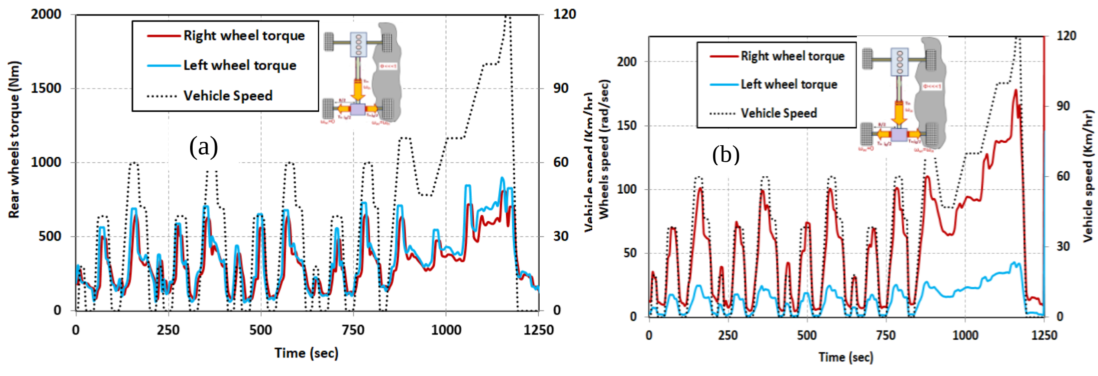

Figure 12: Vehicle wheels torque and speed with the CD with a slippery road.

Figure 13 demonstrates the results of the vehicle wheels torques and speed with the active differential (AD) under a slippery road, the YR and VSS control are applied. When the vehicle right wheels are exposed to a slippery road wet asphalt (μ=0.4) and the left one is exposed to a dry road dry asphalt (Φ=0.8). The AD control avoids the right wheels spinning because for over NEDC more torque is delivered to the left wheels. The rotational speed of the right and left wheels is approximated equal, causing the car to become more stable.

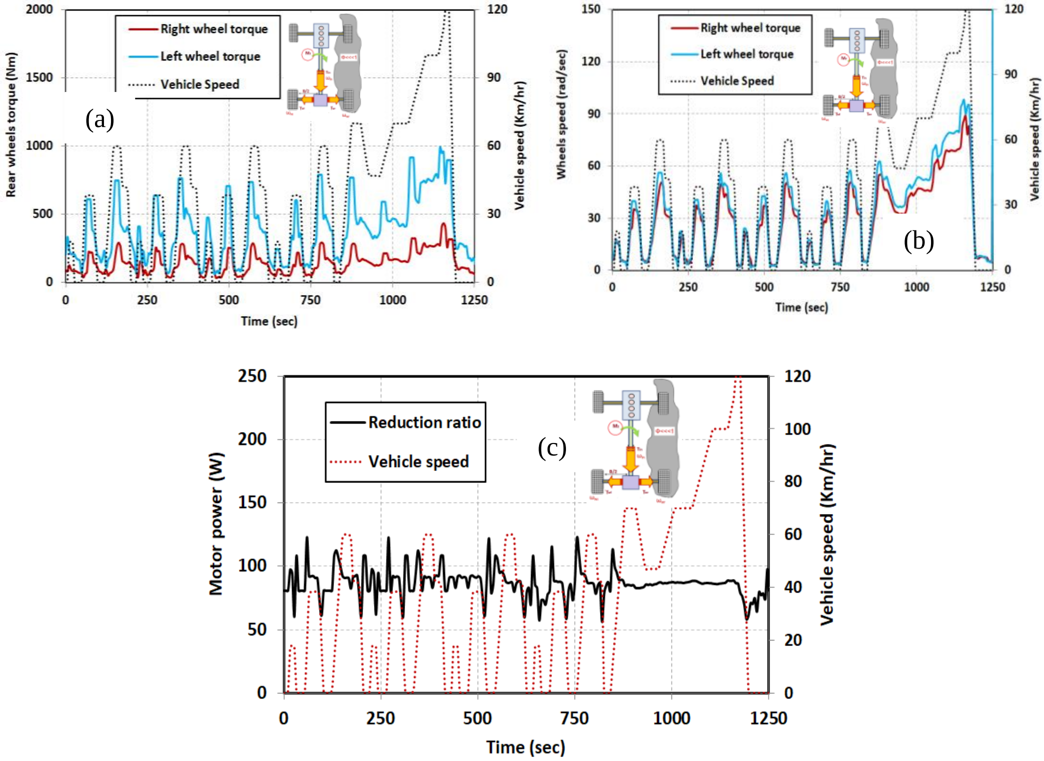

Figure 13: Simulation results of the vehicle wheels torques and speed with the AD with a slippery road.

3.2 Vehicle motion in a left curve

This section's computer simulations are performed at namely J-turn maneuver with constant speeds, to assess the control systems' performance and demonstrate the enhancements brought about by the suggested LQR approach. The simulations involve an automobile cornering during a path following maneuver on a J-turn at longitudinal steady speed V_x=80Km/hr.

Figure 14 shows the results of vehicle responses for the J-turn manoeuvre under uncontrolled, yaw rate (YR) control and integrated YR and vehicle side slip (VSS) control. Referred the step steer analysis, the simulation's chosen steering wheel input angle is depicted in Figure 14(a) and reflects the worst-case situation during collision avoidance. The motorist rapidly shifted the steering wheel from the forward position to the 55^0 position in two seconds. The test result at a dry asphalt road surface (Φ=0.8). Figure 14(b) displays the YR response with three cases control and uncontrolled, where the parameters of the rise time, overshoot, and settle time are all reasonable and the response curves are within the satisfied area with YR control and VSS control, the maximum overshoot at uncontrolled is approximately 20%. Figure 14(c) displays VSS angle response for three cases with control and uncontrolled, where the overshoot is improved and the steady-state error of the system is eliminated at YR+VSS control. Figure 14(d) shows the vehicle lateral velocity, the lateral acceleration are gained at faster response, thus, the vehicle with integrated YR+ VSS control completes its test cycle more quickly. The vehicle with uncontrolled as becomes unstable during this maneuver, and its side-slip angle and YR sharply rise. According to simulation results displayed in Figure 14, the integrated controller performs better in terms of vehicle stability in typical scenarios when the uncontrolled vehicle becomes unstable, but at the expense of a minor drop in longitudinal velocity when compared to the AD integrated YR+ VSS controller. Integrated controllers can maintain the vehicle within safe margins. Figure 15 demonstrates of the vehicle yaw moment and AD torque under uncontrolled, YR control and integrated YR+ VSS control. Figure 15 (a) illustrates the yaw moment (M_Z), the integrated YR+ VSS control needs the lowest moment value, it is observed that maximum peak yaw moment are 835, 1210 and 1560 Nm under an integrated YR+ VSS control, YR control and uncontrolled respectively. This alteration results in a positive peak that matches the wheels' speed. Figure 15 (b) illustrates the AD torque (M_{diff}) related Eq. (10), it is observed that maximum peak AD moment are 385 Nm and 405 Nm under YR control and an integrated YR and VSS control respectively. According to the figures, the uncontrolled vehicle exhibits an undesired oscillatory response with an increasing side-slip angle and yaw moment. Because the responses are very oscillatory and do not resolve to steady-state values at a finite time. The vehicle's dynamic behavior poses a risk. When compared to the uncontrolled vehicle, these data also show that the controllers have significantly enhanced the vehicle's dynamics performance.

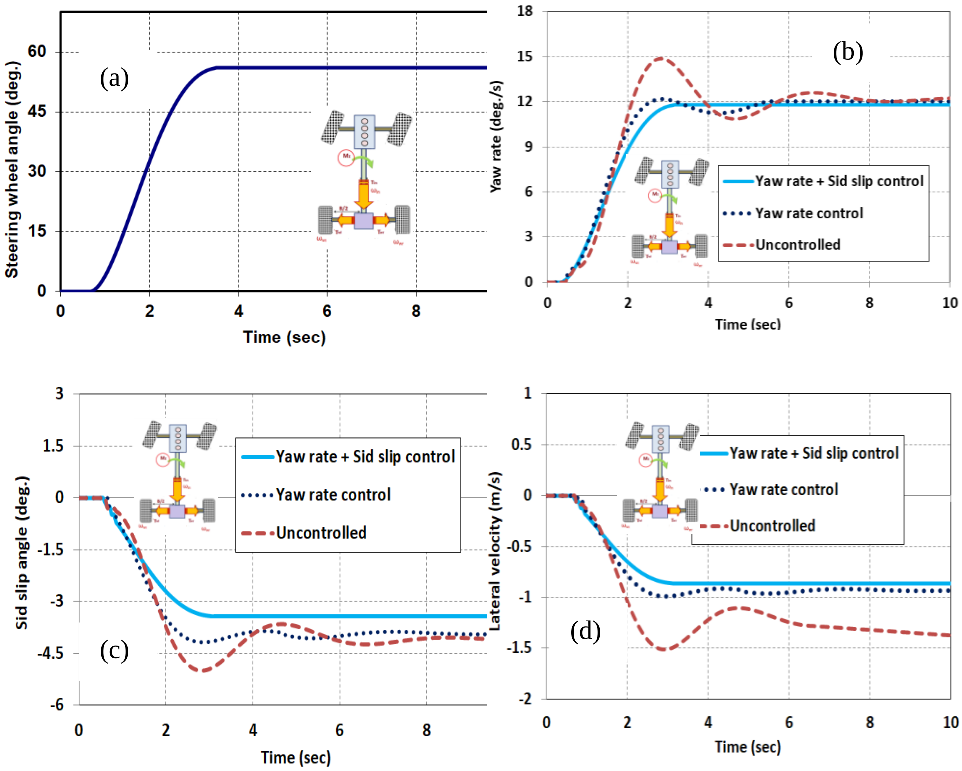

Figure 14: Simulation results of vehicle responses for the J-turn manoeuvre: a. J-turn path input, b. yaw rate, c. side slip angle, d. lateral velocity

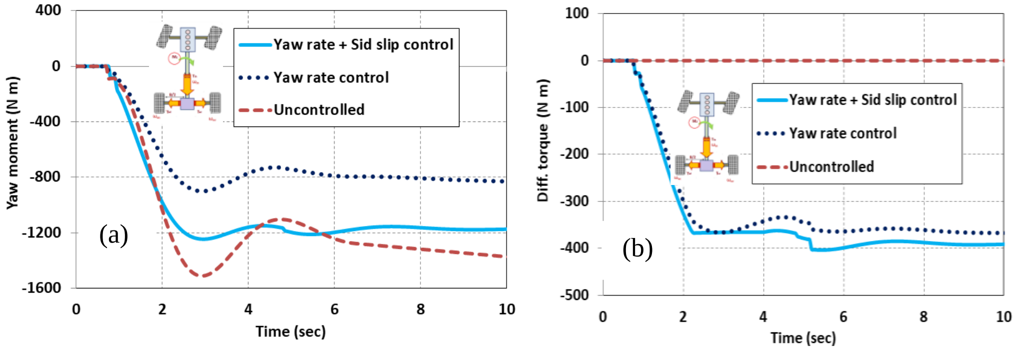

Figure 15: Simulation results with the J-turn manoeuvre: a. yaw moment, b. Active differential torque

Figure 16 and Figure 17 show present the results during the vehicle right wheels are exposed to a slippery road wet asphalt (μ=0.4) and the left one is exposed to a dry road dry asphalt (Φ=0.8), during a path following maneuver on a J-turn at longitudinal steady speed V_x=80 Km/hr.

Figure 16 (a) demonstrates the results of yaw moment with a slippery road; the peak value of yaw moment is 900 Nm at the uncontrolled, 785 Nm at the YR control and 620 Nm at the integrated YR+ VSS control. Demonstrate how both YR control and the integrated YR+ VSS control system effectively manage the unstable reaction in the event of uncontrolled. However, the integrated YR+ VSS control system can enhance the vehicle reaction and minimal side distance, which can follow the intended response, in contrast to the case utilizing yaw control. It can be said that the integrated controller uses less effort to accomplish the goals more effectively. Figure 16 (b) demonstrates the results of AD torque with a slippery road, the maximum of AD torque is 420 Nm with an integrated controller and 338 Nm under YR control.

Figure 17 (a) demonstrates the results of the wheels torque with a slippery road, the peak value of wheels moment is 600 Nm for the right wheel under (ϕ=0.8) and 394 Nm for the left wheel (ϕ=0.4) with the integrated YR+ VSS control. Figure 17 (b) demonstrates the results of the wheels speed with a slippery road, the peak value of left wheel speed is 68 rad/s for inner wheels, and 62.8 rad/s for the right wheel with the integrated YR+ VSS control, the steady state speed of inner wheels is 40 rad/s and outer side is 58.6 rad/s.

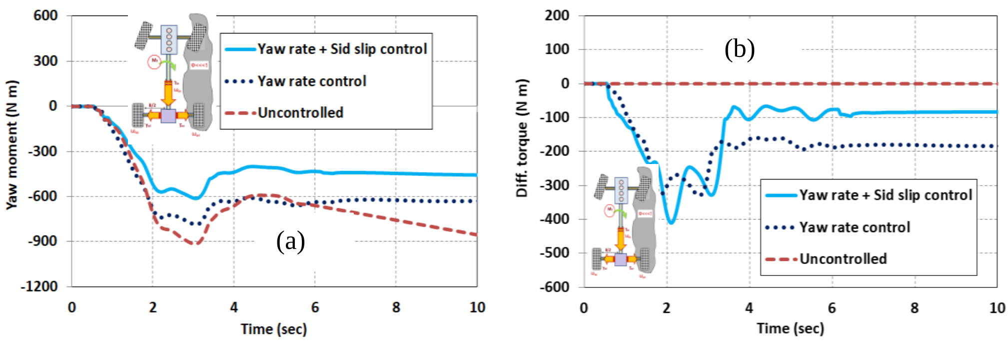

Figure 16: Simulation results with a slippery road: a. yaw moment, b. Active differential

torque

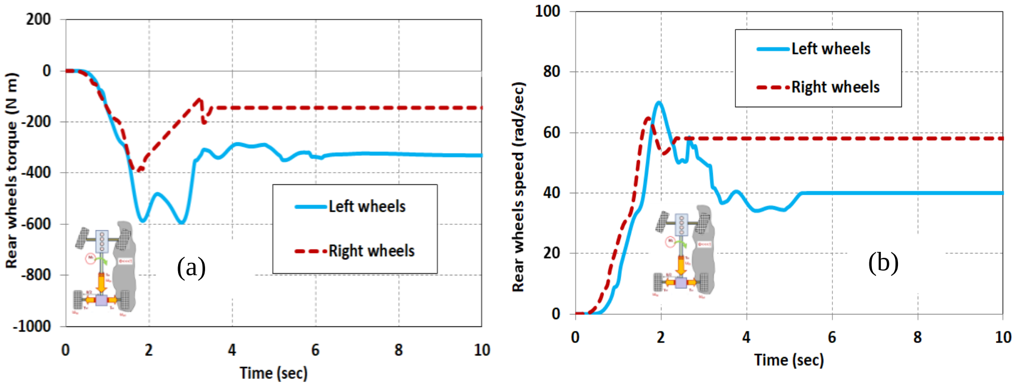

Figure 17: Simulation results with a slippery road: a. wheels torque, b. wheels speed

4 CONCLUSION

This study suggests an active differentials (AD) system with integrated yaw rate (YR) and vehicle side slip (VSS) control to enhance the stability and handling of vehicles. This investigation allows for the deduction of the following conclusions.

- The proposed configuration of the vehicle drive train model with AD is presented, applying the different parameters to the AD mathematical model with two electromechanical actuators.
- The usefulness of the suggested controller is investigated using MATLAB/Simulink in a variety of driving scenarios, including straight lines under NEDC and J-turns with different road adhesions, to regulate lateral slide slip and vehicle YR on different road adhesions can be obtained by an LQR controller.
- The combined control of YR and VSS control is the foundation for an LQR control system for vehicle lateral stability. To produce the corrective yaw moment, a strategy for the AD torque distribution of wheels is designed. The AD torque distribution strategy is developed to generate the corrective yaw moment.
- The peak value of wheel moment is 600 Nm for the right wheel under (ϕ=0.8) and 394 Nm for the left wheel (ϕ=0.4) with the integrated YR and VSS control, it can be said that the integrated controller uses less effort to accomplish the goals more effectively.
- According to simulation results, the vehicle with the suggested AD with a stability control system, which consists of YR and VSS by an LQR, can effectively follow the specified vehicle YR and VSS angle trajectories. It also performs better than the standard Uncontrolled or YR one because YR and VSS lessen the lateral displacement a side force brings.
- The YR undershot and overshot have been somewhat reduced. Additionally, it is anticipated that the vehicle's dynamic reaction and tracking capabilities performance will show promise. The AD with YR and VSS driver assistance system is effective in improving vehicle stability, reducing steering effort, and lane-tracing performance.

REFERENCES

[1] Abe, M., Kano, Y., Suzuki, K., Shibahata, Y., and Furukawa, Y. Side-slip control to stabilize vehicle lateral motion by direct yaw moment. JSAE Rev., 2001, 22(4), 413–419.

[2] E.S. Mohamed, M.I. Khalil and A.A.A. Saad. 2019. Analysis of Synchronous Moment for Active Front Steering and a Two Actuated Wheels of Electric Vehicle Based on Dynamic Stability Enhancement, Int. J. Vehicle Structures & Systems, 11(1), 88-101. doi:10.4273/ijvss.11.1.17.

[3] Shuibo Z. et AL. Controller design for vehicle stability for vehicle stability, Control engineering practical, 14 (2006) 1413-1421.

[4] A.S. Emam and E.S. Mohamed. 2021. Enhancement of Anti-Lock Braking System Performance by using Intelligent Control Technique for Different Road Conditions, Int. J. Vehicle Structures & Systems, 13(1), 37-45. doi:10.4273/ijvss.13.1.09.

[5] Ahmed Shehata Gad, Eid S. Mohamed, and Samir M. El-Demerdash "Effect of Semi-active Suspension Controller Design Using Magnetorheological Fluid Damper on Vehicle Traction Performance' SAE, 2020-01-5101

[6] Baslamisli, S. C., Kose, I. E., and Anlas, G. Gainscheduled integrated active steering and differential control for vehicle handling improvement. Vehicle Syst. Dyn., 2009, 47(1), 99–119.

[7] Eid S. Mohamed, and Saeed A. Albatlan (2014), "Modeling and Experimental Design Approach for Integration of Conventional Power Steering and a Steer-By-Wire System Based on Active Steering Angle Control." American Journal of Vehicle Design, vol. 2, no. 1 (2014): 32-42. doi: 10.12691/ajvd-2- 1-5.

[8] B Mashadi, S Mostaani, M Majidi "Vehicle stability enhancement by using an active differential" Proceedings of the Institution of Mechanical Engineers, Part I: Journal of Systems and Control Engineering 2011, 225: 1098, https://doi: 10.1177/0959651811405113.

[9] Cheli F., et al., A New Control Strategy for A Semi-Active Differential (Part I), 16th IFAC World Congress, 2005

[10] Diachuk, M.; Easa, S.M. Improved Mathematical Approach for Modeling Sport Differential Mechanism. Vehicles 2022, 4, 74–99. https://doi.org/10.3390/vehicles4010005

[11] Shibahata Y., Shimada K., Tomari T., Improvement of Vehicle Maneuverability by Direct Yaw Moment Control, Vehicle System Dynamics Vol. 22, 1993

[12] M. Terzo, Employment of Magneto-rheological Semi-active Differential in a Front Wheel Drive Vehicle: Device Modelling and Software Simulations, SAE Technical Papers 2009-24-0130, 2009, http://dx.doi.org/10.4271/2009-24-0130.

[13] A. Lanzotti, et al., Design and development of an automotive magnetorheological semi-active differential, Mechatronics 24 (5) (2014) 426–435.

[14] Antonio L. et al., Design and development of an automotive magnetorheological semi-active differential, Mechatronics 24 (2014) 426–435.

[15] Federico C. et al., A new control strategy for semi-active differential (part I) All rights reserved 16th Triennial World Congress, Prague, Czech Republic, 2005 IFAC.

[16] Behrooz M. et al., Vehicle path following control in the presence of driver inputs, Proc IMechE Part K: J Multi-body Dynamics 227(2) 115–132.

[17] Riccado M et al.,] "Detailed and reduced dynamic models of passive and active limited-slip car differentials" Mathematical and Computer Modelling of Dynamical Systems, 12, No. 4, ust 2006, 347 – 362.

[18] C Ghike, T Shim, and J Asgari "Integrated control of wheel drive–brake torque for vehicle-handling enhancement" Proc. IMechE , Part D: J. Automobile Engineering, 223, 4, 2009, 439-457.

[19] Julio E et al., Mobile robot path tracking using a robust PID controller, Control Engineering Practice 9 (2001) 1209–1214.